Article:

Bradley, D, Lawes, M and Morsy, ME (2021) Combustion-induced turbulent flow fields in premixed flames. Fuel, 290. 119972. ISSN 0016-2361

https://doi.org/10.1016/j.fuel.2020.119972

Combustion - Induced Turbulent Flow Fields in Premixed Flames

D. Bradley[b], M. Lawes[b], M. E. Morsy[a,b,*]

[a] Faculty of Engineering at El-Mattaria, University of Helwan, Cairo 11718, Egypt.

[b]Institute of Thermofluids, School of Mechanical Engineering, University of Leeds, LS2 9JT, UK.

*Corresponding author: M_Morsy@m-eng.helwan.edu.eg.

Abstract

Combustion-induced turbulence is studied in explosions of methane/air in a steel sphere with optical access. Rms turbulent velocities, u', created by four peripheral variable speed fans, were measured by Particle Image Velocimetry, PIV, which indicated near-uniform, isotropic turbulence, with small mean velocities. A near-spherical propagating flame, and the gaseous expansion generated a radially outwards velocity of unburned mixture, the intensity of which depended upon the burning velocity and volume increase due to combustion. The study is to measure any extra turbulence created by this outwards velocity pulse. Only wave lengths less than the flame circumference can wrinkle the flame and increase the burning velocity, u_t. Consequently the effective rms velocity at the flame front affecting its propagation,, u'_k, less than u'. Analysis shows, u'_k, to be a function of flame radius. The velocity pulse generated additional turbulence, enhancing u'_k. This enhanced u_t , giving further positive feedback. This higher rms value is designated as a spatial rms turbulent velocity, u'_s. PIV-measured gas velocities are resolved into a mean radial velocity, $\overline{U}_r$ and, u'_s, with their radial profiles. These are derived from explosions at different equivalence ratios, pressures, and temperatures. At the radii at which u_t are measured, u'_s/u'_k is enhanced by the high rates of burning and volumetric expansion. This ratio attained a high value of 2.5, with stoichiometric CH_4/air. Values of u_t measured in explosions are higher than those measured in steady-state burners, attributable to the induced u'_s, enhancing u_t, in explosions, with no such effect in burners.

Keywords: Combustion generated turbulence, Burning velocity, Premixed explosions, Turbulent burning.

Nomenclature

$\bar{c}$	mean reaction progress variable
$\bar{k}_\eta$	dimensionless wave number
L	turbulent integral length scale
n_k	number of integral length scales
P	pressure
r_f	flame radius for equal volumes
r_m	maximum flame radius, (=60 mm)
R_λ	Reynolds number, based on the Taylor scale λ
t	time
T_P	burned gas temperature
T_u	initial temperature
S_t	turbulent flame speed
$\bar{S}(\bar{k}_\eta)$	non-dimensional power spectral density
u_l	laminar burning velocity
u_t	turbulent burning velocity
U_r	radial velocity component at each (x, y) grid node
$\bar{U}_r$	mean radial velocity
$\bar{u}_g$	mean gas velocity
u'	rms turbulent velocity
u'_k	effective rms turbulent velocity, acting on flame
u'_s	spatial rms turbulent velocity acting on flame
f	fan speed
φ	equivalence ratio
η	Kolmogorov scale
λ	Taylor scale of turbulence
ρ_b	burned gas density
ρ_u	unburned gas density

1. Introduction

Since the early days of combustion science there has been an interest in combustion turbulence, namely the turbulence generated by combustion. Advances in diagnostics, particularly Particle Image Velocimetry, PIV, have greatly facilitated experimental studies of such generation. Vessels with fan-stirred mixing of the contents, that create near-uniform, isotopic turbulence, are often employed to study the effect of turbulence upon chemical reactions and phase changes, and the measurement of turbulent burning velocities [1-3]. Peters [4] has shown that radial flame propagation will change the original cold flow turbulence and Lawes [5] has employed single point Laser Doppler Anemometry, LDA, to measure the velocity of unburned gases ahead of a turbulent flame.

However, LDA, unlike PIV, does not provide information on the spatial structure of the flow, comparable to that provided by, PIV, which is able to provide a detailed temporal evolution of the flow velocity at the measurement plane. It can also provide data on the mean velocity, higher-order moments, and frequency spectra, with high accuracy. It has recently been used by the current authors to characterise the cold flow turbulence, in the Leeds fan-stirred vessel, in the absence of chemical reaction. This revealed good levels of uniformity and isotropy [6]. Spherical explosions, as a result of the combined influences of a high burning rate and high volumetric expansion can generate a strong outwards velocity pulse ahead of the flame. The present experimental study focuses on whether this strong velocity pulse of outwards velocity is able to generate additional “combustion turbulence” and, if so, to quantify its magnitude.

As will be shown, the technique has been developed further, to characterise the large radial expansion velocities that are generated ahead of the flame by combustion in centrally ignited, radial, explosions, and their interaction with the turbulence created by the fans. Closed vessel explosions, through the associated gaseous expansion, generate a powerful velocity pulse that is related to the rate of combustion and volumetric expansion. Interactions of the high velocity wave further enhance the turbulence, that, in turn, further accelerates the oncoming flame. The development of this interaction is a motivating aspect of the present study.

To this end, The paper reports comprehensive velocity measurements in methane/air mixtures, with initial rms turbulence velocities, u', of up to 4 m/s and, equivalence ratios, φ, = 0.8, 1.0 and 1.3, at 300 K and 400 K, and pressures of 0.5 and 1.0 MPa. In the measurement of turbulent burning velocity, u_t, allowance must be made for the changes in the effective rms turbulence velocity, to which the explosion flame is exposed [2]. In the earlier stages of a turbulent spherical explosion, the flame surface is wrinkled only by length scales smaller than the flame circumference. If $u'$is the cold mixture rms turbulent velocity, then the effective rms velocity for flame surface wrinkling, u'_k, must be less than this. The ratio, $u'_k/u'$is found by integrating the non-dimensional power spectral density, $\bar{S}(\bar{k}_\eta)$, over the range of relevant wavelengths. Based on an original study of Abdel-Gayed et al. [2], Bradley et al. [1] derived the ratio $u'_k/u'$from:

$$\frac{u'_k}{u'} = \left[\frac{15^{0.5}}{R_\lambda}\int_{\bar{k}_{\eta 1}}^{\bar{k}_{\eta 2}} \bar{S}(\bar{k}_\eta)d\bar{k}_\eta\right]^{1/2}, \tag{1}$$

where R_λ is the Reynolds number, based on the Taylor scale λ, and $\bar{S}(\bar{k}_\eta)$ is the non-dimensional power spectral density, expressed in terms of $\bar{k}_\eta$, a dimensionless wavenumber, obtained from the wavenumber multiplied by the Kolmogorov length scale, η. $\bar{S}(\bar{k}_\eta)$ is given by [1]:

$$\bar{S}(\bar{k}_\eta) = \frac{0.01668R_\lambda^{2.5} + 3.74R_\lambda^{0.9} - 70R_\lambda^{-0.1}}{1 + \left(0.127R_\lambda^{1.5}\bar{k}_\eta\right)^{5/3} + \left(1.15R_\lambda^{0.622}\bar{k}_\eta\right)^4 + \left(1.27R_\lambda^{0.357}\bar{k}_\eta\right)^7}, \tag{2}$$

The limits $\bar{k}_{\eta 1}$ and $\bar{k}_{\eta 2}$, in Eq. (1)represent the smallest and largest possible wavelengths conveniently expressed by $n_k L$, where n_k is the number of integral length scales and L is the integral length scale (= 20 mm) [6], as:

$$\bar{k}_{\eta k} = \frac{2\pi\eta}{n_k L} = \left(\frac{32\pi}{15^{0.25}n_k}\right)R_\lambda^{-1.5}. \tag{3}$$

The lower limit $\bar{k}_{\eta 1}$, in Eq. (1) is assumed to be the flame diameter, D_f $(= 2r_f)$, as it is based on the maximum wavelength, $n_k L$, that can wrinkle the flame. In the case of explosions, the upper limit $\bar{k}_{\eta 2}$ depends upon the size of the smallest eddy that can be chemically acting on the flame during its lifetime. In the present study, the lower limit, $\bar{k}_{\eta 1}$, corresponds to the maximum possible wavelength, which occurs when the flame approaches the internal diameter of the vessel, namely 380 mm. The upper limit, $\bar{k}_{\eta 2}$, corresponds to the smallest wavelength, taken to be the Kolmogorov scale, η. Consequently, $n_k L$ in Eq. (4) is η and $\bar{k}_{\eta 2}$ is 2π. Figure 1 shows the development of u'_k/u' with r_f for stoichiometric CH_4/air at 300 K and 0.1 MPa for three different values of u'. For the present experimental, $u'$is related to the fan speed rpm, f, by [6]:

$$u' = 0.00124f \quad (\text{m/s}). \tag{4}$$

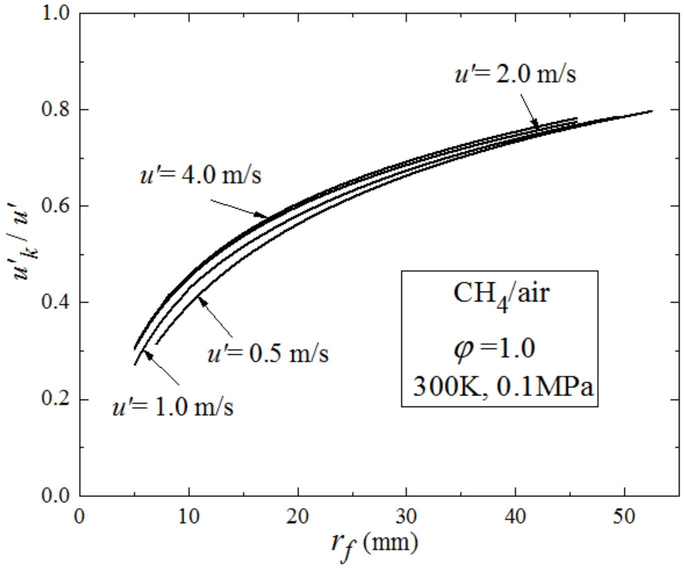

Fig. 1. Development of u'_k/u' with r_f.

During an explosion, PIV-measured gas velocities are resolved into a mean radial velocity, $\overline{U}_r$ and, u'_s, the spatially effective rms turbulent velocity. To calculate it from the PIV measurements, a zone of specified thickness, ~ 1 mm ahead of the flame front, is defined. Within this zone, the radial velocity profile, surrounding the flame front, is deduced and divided into a number of circumferential sectors, N_i. The spatial rms turbulent velocity, u'_s, was then calculated for each sector and averaged over the velocity profile around the flame front from:

$$u'_s(x,y) = \frac{1}{N_i}\sum_{i=1}^{N_i}\left[\sqrt{\left(\frac{1}{N_v}\sum_{v=1}^{N_v}\left[U_r(x,y) - \bar{u}_g(x,y)\right]^2\right)}\right]. \tag{5}$$

Here U_r is the radial velocity component at each (x,y) grid node, and $\bar{u}_g$ is the mean gas velocity within each sector. N_v is the total number of velocity vectors in each sector. Importantly, u'_s is not only influenced by the spectrum of turbulence but, as will be shown, it is also affected by any turbulence generated by the velocity field created ahead of the flame by the combustion process.

The calculation of $U_r\ (x, y)$ was executed in three steps, using a series of MATLAB scripts. The first detects the flame front, and converts it into, (x, y), Cartesian coordinate. The second is to match the flame front coordinates with the nearest unburned gas velocity measurement. The final step is to calculate the radial velocity component,$U_r(x, y)$, from which u_s' is calculated in Section 5. The polar transformation of the velocities starts from the determination of the global centre $(x_c,\ y_c)$, which indicates the spark position. The local angle of each velocity, around the flame front, is then calculated from:

$$\theta = \arctan\{(y - y_c)/(x - x_c)\}, \tag{6}$$

with the radial velocity calculated from the velocity components in:

$$U_r(x, y) = u(x, y)\cos(\theta) + v(x, y)\sin(\theta). \tag{7}$$

Here a positive value of $U_r(x, y)$ implies an outward direction, $u(x, y)$ is the velocity component in the x-direction and $v(x, y)$ the velocity component in the y-direction.

2. Methodology

Measurements were made in the Leeds fan-stirred vessel of spherical stainless steel, with an inner radius of 190 mm, and three pairs of optically flat quartz windows of 150 mm diameter. These allowed full visualisation of the central region of the vessel and the flame propagation at essentially constant pressure. Each of the four identical fans is powered by an 8 kW three phase electric motor, was located close to the wall of the vessel. The fans were arranged in a regular tetrahedron configuration, in an attempt to optimise homogenous, isotropic turbulence. Their speed was controlled by individual solid state variable frequency convertors, within a control range of 200-10,000 rpm (3.3-176 Hz), in increments of 20-30 rpm. Further details of the vessel and comprehensive characterisation of the non-reacting, single phase, turbulent flow can be found in [6].

A high repetition rate double pulsed Nd:YAG laser (DM60-DH, Photonics), generated pulses of 12 mJ at a wavelength of 532 nm at 5 KHz. The laser beam expanded into a vertical sheet of about 1.0 mm thickness, passing through the centre of the vessel. Here it uniformly illuminated the dispersed 1 µm diameter seeding particles of olive oil, generated by six jet atomisers (9010F0021, DANTEC). The measuring system comprised two spherical lenses of -300 mm and 650 mm focal lengths, and a cylindrical lens of-20 mm focal length. Laser pulses, were synchronized with a high-speed camera perpendicular to the laser sheet, to record a 12-bit image pair of (1024×1024 pixels), under the control of Dantec dynamics studio software. An adaptive algorithm was employed to process images. This algorithm is an iterative and automatic way of calculating velocity vectors, based on the seeding particle density. A minimum interrogation area of (8×8 pixels) and a maximum of (32×32 pixels) were employed, with a magnification ratio of 0.117 mm/pixel. More details of the PIV system and adaptive algorithm appear in [7].

It is advisable to image as large an area as possible, in order to ascertain how the flame front propagation develops in its interaction with the turbulent flow field. Bearing in mind the distance to the vessel wall, the window diameter, and the capture angle of the lens, the maximum area that could be physically imaged at the central plane of the vessel was a region 150 mm square. However, due to the finite resolution of the camera (1024×1024 pixels), this would result in poor spatial resolution of the measured velocity fields. It was therefore, necessary to establish the maximum possible spatial resolution of the turbulent structures and their flame interactions, while also preserving information of bulk-flow behaviour.

The integral scale of turbulence, L, is about 20 mm [6], indicative of a relatively large scale flow structure, relative to the flame brush thickness. The Taylor microscale, λ, under atmospheric conditions, is respectively, 2.24 mm, 1.53 mm and 0.71 mm, respectively, for u' values of 1, 2 and 4 m/s. The Kolmogorov length scale, η, was calculated to be between 0.18 mm and 0.07 mm in the u' range of 1 - 4 m/s. The minimum possible interrogation area size, which could be used in conjunction with the PIV adaptive method without excessive loss in accuracy, was 8 (~0.94 mm) pixels square. This is about 5-12 times larger than η. Clearly, it is not possible to capture the velocity fluctuations associated with η, whilst also recording the larger scales, between L and λ.

Consequently, key characteristics were centred around the integral scale, L, of 20 mm, a value of, u_l, of 0.358 m/s, for stoichiometric methane/air at atmospheric conditions [8], an inner reaction zone thickness of 0.75 mm and an rms turbulent velocity u', of between 1 and 4 m/s. Combustion then occured in the corrugated flamelet region of the Borghi diagram [9]. Here the influence of turbulence scales larger than the flame thickness are the more important. For this reason, an area of interest larger than the integral length scale is embraced, in conjunction with an interrogation area size around the same size as λ. Based on this, a square area of 120×120 mm^2 was selected. The duration of each experiment was about 30 ms, at a frequency of 5 kHz. This ensured capture of turbulent motion in the key range between λ and L, the most controlling influences upon flame structure.

3. Velocity field in explosions

Figure 2 shows the velocity vector maps, measured during explosions of stoichiometric CH_4/air at an initial pressure of 0.1 MPa, and an initial temperature of 300 K with u' = 1, 2 and 4 m/s. The same vector colour code, shown on the right of Fig. 2, is used for all values of u'. Flame contours are shown at several elapsed times after ignition. One representative experiment of five is shown, at each value of u'. Such figures show the interaction between the unburned flow field and the flame front. As u' increases, the propagation of the flame changes from a loosely spherical nature, at u' = 1 m/s, to one that is more highly deformed and convoluted, at u' = 4 m/s. Clearly, the flow structures before each ignition are highly variable, as is the response of the flame front to them, with some sections of the flame initially moving away from the point of ignition. These sections can drag the flame front along with them, giving the appearance of rapid flame propagation in that direction. This is clear with u'= 4 m/s. In contrast, where the bulk cold flow moves towards the flame, burned gas flame propagation is noticeably arrested. Clearly, the response of the flame to the flow movement, is due to the relative difference between the burning velocity of the mixture and the flow velocity ahead of the flame.

The local changes in flow velocity are significantly higher than those in burning velocity. As a result, the flow wrinkles the flame front before a particular flow structure is consumed by the flame. With u' = 1.0 m/s, the flow velocity is small and the flame front is only slightly wrinkled. As u' increases, the flame is distorted and moved by the flow, with wrinkling and stretching of the flame front, as it departs from its original nearer-spherical nature. For all values of the rms velocity, as the flame propagates, the velocity of the unburned gas ahead of it is being forced outwards, by the expanding burned gases. This phenomenon is most noticeable at u' = 1.0 m/s, due to the relatively slow moving flow field structures, but it is still evident at u' = 4.0 m/s. This is indicative of the symbiotic relationship between the flow structures contained within the reactants, and the propagating flame front. The flame is affecting the structure of the flow, and the flow is affecting the structure of the flame.

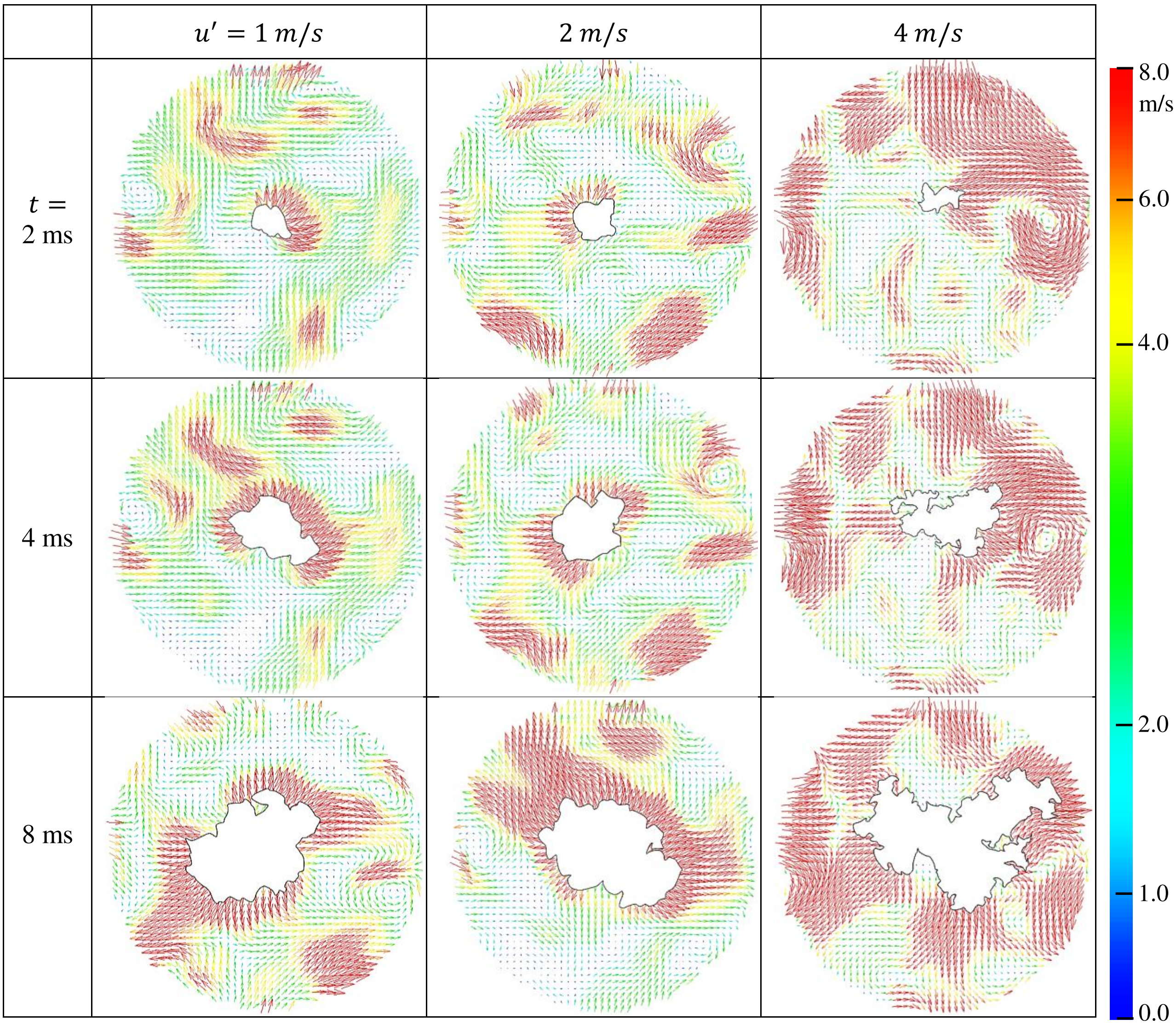

Fig. 2. Development of CH_4/air turbulent flames, with φ =1.0 at 0.1 MPa and 300 K, for u' = 1, 2 and 4 m/s.

4. Combustion mean and rms velocities

The lower fluctuations in Fig. 3a are those in the local mean radially outwards velocity, U_r, just ahead of a stoichiometric CH_4/air flame front, at atmospheric pressure at t = 2.4 ms, after ignition. The small flame front shows few wrinkles, as it is exposed to but a small part of the full spectrum of turbulence. This phenomenon is also clearly seen in the velocity vectors fields, in Fig. 2, in which small wrinkles move faster, and increase the unburned gas exposure significantly. As time passes, the flame front grows, and the front becomes affected by small to progressively larger scales. This can be seen in Fig.

3b, from the increasing the fluctuations of radial velocity, and flame front wrinkling, after 8.6 ms. There are consequent increases in the turbulent burning velocity.

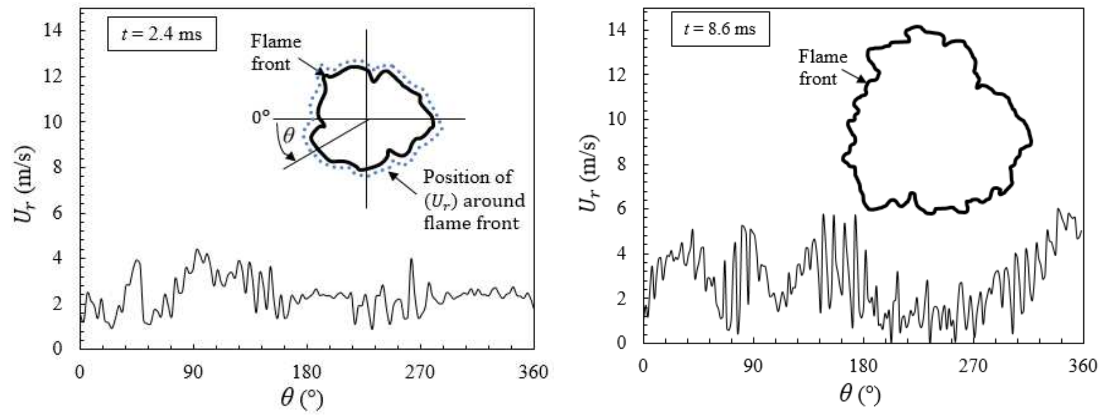

(a) (b)

Fig. 3. Local mean radial velocity, U_r, around the flame front, for stoichiometric CH_4/air mixture, u'= 1.0 m/s, 300 K and 0.1 MPa , at (a) t = 2.4 ms (r_f = 14 mm), and (b) t = 8.6 ms (r_f = 30 mm).

The all-important measured radial variations of the mean gas velocities, $\overline{U}_r$, of the unburned mixture ahead of the flame radial are shown, at three different times after ignition in Fig. 4. The three times were 4, 8 and 12 ms, with again, a stoichiometric CH_4/air flame, at atmospheric pressure, and 300 K, with u'= 1 m/s, and gas velocity measurements up to a radius of 60 mm. The local radial velocity, $U_r(x,y)$, was first identified at each grid node within an annulus area of thickness~ 1 mm, around the flame front, and averaged over the entire circumferential area, to yield, $\overline{U}_r$. The calculation started at the tip of the leading edge of the flame front, moving radially outwards from there. The velocity profile before ignition is also shown. As a turbulent flame develops from a point ignition source, the flame propagation is laminar-like, as shown from the velocity profile at t = 4 ms. As the flame grows, the turbulent flame speed increases, along with $\overline{U}_r$.The strong velocity pulse that is generated, moving ahead of the flame is apparent.

The corresponding radial rms velocity profiles for the same three time intervals, are shown in Fig. 5. Values of the rms velocity were calculated for the same annulus areas, moving from the flame tip towards the window edge. As the flame propagates, the flame front is exposed to an increasing range of turbulent wave lengths and, as a result, the rms velocity acting on the growing flame front increases. It might also be anticipated that the strength of the velocity impulse generated ahead of the flame is related to both the rapidity of the combustion, and the magnitude of the associated increase in volume. Any associated generation of turbulence would augment u'_k, increasing the value of u'_s/u'_k. Consequently, the influences of changes in φ, temperature, and pressure upon u'_s were investigated, using CH_4/air mixtures.

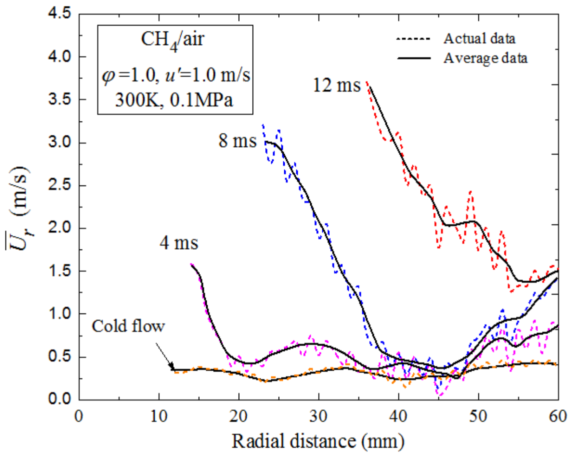

Fig. 4. Variation of mean radial gas velocity, $\overline{U}_r$ with the radial distance.

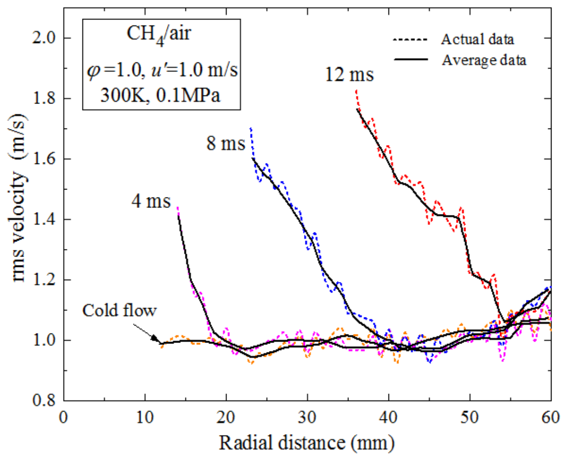

Fig. 5. Variation of spatial rms velocity with the radial distance.

To study further the effect of different enhancements of the velocity impulse generated by the flame on the enhancement of u'_s further, changes in φ, temperatures, and pressures of CH_4/air mixtures were investigated. The results are shown in Figs. 6. and 7. Again this involved the study of radial profiles of u'_s, this time normalised by u', plotted against r_f/r_m. In Fig. 6 the vertical line at r_f/r_m= 0.2 marks the limit of the zone within which ignition and its associated reactions occur. Here, there is a transition from an igniting plasma to a propagating flame, with developing turbulence.

This involved the measurement of flame speeds and u'_s/u'as a function of φ = 1.0 and 1.3, temperatures of 300 and 400 K, and pressures of 0.1 and 0.5 MPa. The PIV measured vectors around the flame front were processed at each instant during the evolution of the flame, enabling u'_s to be calculated. This was repeated for u'= 0.5, 1.0, 2.0 and 4 m/s. Figs. 6 and 7 cover stoichiometric CH_4/air, at 300 K and 0.1 MPa. In addition. Fig. 6 covers 400 K, 0.1 and also 0.5 MPa, and 300 K. Fig. 7 also covers CH_4/air with φ = 1.3 at 300 K and 0,1 MPa. Each curve in a figure represents mean values from five explosions. For all values of u', the value of u'_s/u'increases with r_f/r_m.

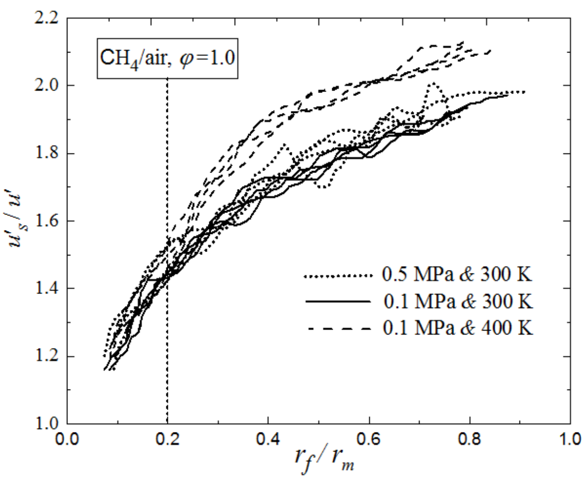

Fig. 6 Influence of pressure and temperature on u'_s.

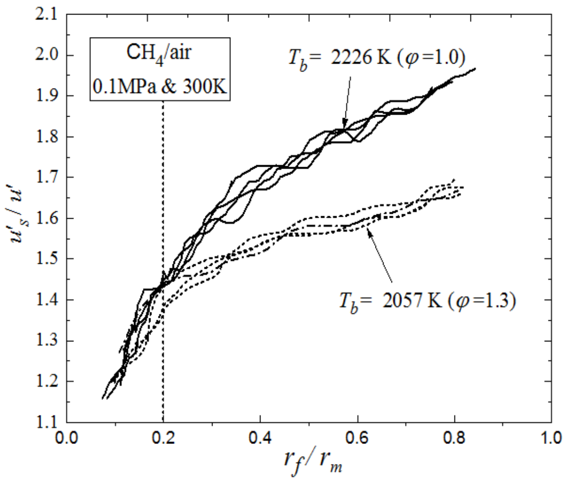

Fig. 7. Influence of equivalence ratio on u'_s. T_b is burned gas temperature.

Figure 6 shows little effect of pressure, but at the higher initial temperature of 400 K, higher values of u'_s/u' develop with increasing radius. In Fig. 7, T_b is the adiabatic temperature of the burned mixture. The stoichiometric mixture had the higher adiabatic temperature and higher flame speed/. The slower burning, less expansive, $\varphi = 1.3$ mixture, generates the lowest values of u'_s/u'. Both figures confirm that both a higher burn rate and a higher volume increase u'_s/u'.

The overall quantitative findings from Figs. 7 and 8 can be empirically correlated by the following relationship:

$$u'_s = \left[\frac{1 - 0.49\, ln(r_f/r_m)}{280}\right].f.\left(\frac{T_u}{T_0}\right)^{0.81}\left(\frac{P}{P_0}\right)^{0.01}\left(\frac{\varphi}{\varphi_0}\right)^{a}. \tag{8}$$

Here $r_f$is the mean flame radius, $f$the fan speed in rpm, T_u and P are the initial temperature and pressure, respectively, $T_0 = 300\ K$, $P_0 = 0.1\ MPa$, φ_0=1.0.Where a =0.36 for$\varphi < 1.0$ and $a = -0.55$ for $\varphi > 1$. Eq. (8) can be used to quantify the spatial rms velocity,u'_s, ahead of turbulent methane flames at pressures, up to 0.5 MPa.

5. Turbulence created by the velocity pulse

Figs 6 and 7 clearly show u'_s/u' to increase as the flame propagates outwards. The value of u' is determined solely by the speed of the fans and is an asymptotic value for the flame. The enhanced turbulence cannot be directly generated solely by the velocity pulse, because, in the absence of fan-generated turbulence, in a laminar explosion, no turbulence is created ahead of the flame. From Figs. 4 and 5 it can be seen that turbulence intensities, measured by $u'_s/\overline{U}_r$, are at their highest at the smaller radii. The enhancement of the turbulence would appear to originate directly at the wrinkled flame front, and be attributable to the existing turbulence beyond that front. In Section 5 it is suggested that a stronger velocity impulse, arising from both a high burning velocity and a high volumetric expansion might increase the value of $\frac{u'_s}{u'}$, and this is supported by Figs. 6 and 7. Bearing in mind that u' is constant during a single explosion these results show u'_s to be increasing by such a mechanism, albeit at a diminishing rate, throughout the explosion.

This view is more directly assessed in Fig. 8., which plots u'_s/u'_k against r_f/r_m, throughout explosions for a variety of velocity pulses of different strengths. Throughout the explosion, higher values of u'_s/u'_k are generated by mixtures of higher reactivities. The highest values of u'_s/u'_k are generated by the most reactive and most expansive mixture, that of stoichiometric CH_4/air at 400 K. and 0.1 MPa. The lowest values of u'_s/u'_k occur with the least reactive and least expansive mixture, that of CH_4/air, with $\varphi = 1.3$ at 300 K and 0.1 MPa. Figs 6 and 7 show u'_s to be increasing throughout the explosion. There is an interesting interplay between u'_s and u'_k. Fig. 1 shows u'_k to increase throughout the explosion. From Fig. 8, it is clear that, for these explosions, the increases in u'_k must be greater than those in u'_s. For the large flame radii (0.2 > r_f/r_m> 0.7), u'_s can be correlate with u'_k by:

$$(u'_s/u'_k) = -1.18\,(r_f/r_m) + 2.61. \tag{9}$$

Hence, the effective rms turbulent burning velocity based on the power spectral density, u'_k, can still be used with the correction factor proposed in Eq. (9). During the early transition to a propagating flame up to r_f/r_m = 0.2, there is a sharp change in u'_s/u'_k. Later, in the regime where turbulent burning velocities are measured, the spatial rms turbulent velocity acting on flame is about 2.5 u'_k, for stoichiometric CH_4 mixtures, and about 2.2 for mixtures with $\varphi = 1.3$.

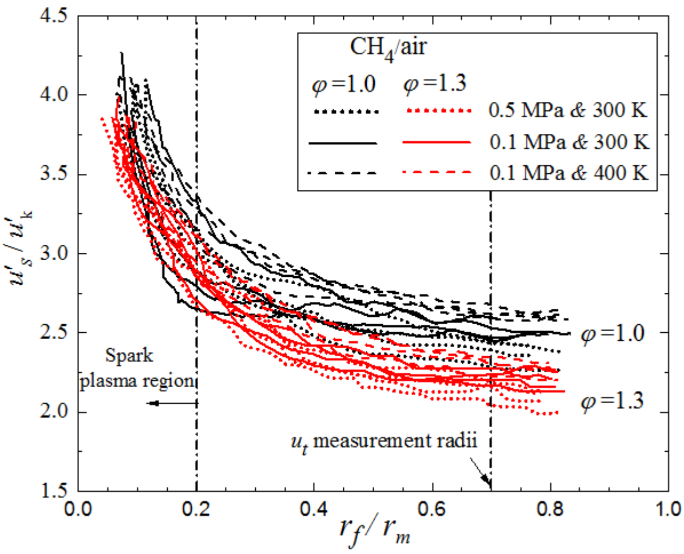

Fig. 8. Variation of u'_s/u'_k with r_f/r_m, for stoichiometric and rich methane.

6. Burning velocities: Comparisons with some burner results

To be meaningful, a burning velocity, u_t, requires an associated area. A practical rational for the selection of such an area is that, when multiplied by the burning velocity and the appropriate density, it yields the mass burning rate. A convenient approach is to balance the volume of burned gas outside a spherical surface of radius, r_f, with the volume of unburned has inside it [10, 11]. In spherical flame propagation, the mass burned can be regarded as contained within the sphere of radius r_f with a density ρ_b, and a mass burning rate of $4\pi r_f^2 u_t \rho_u$. Balancing this with the rate of accumulation of burned gas yields:

$$u_t = (\rho_b/\rho_u)\, dr_f/dt \qquad (10)$$

Other surfaces might be selected [12]. For example, standardistion of measurements might be achieved through a particular value of the reaction progress, $\bar{c}$. With a spherical flames the surface area is large, at low $\bar{c}$, but with a conical flame the surface area is large, at high $\bar{c}$.

As in [11] Mie scattering from very fine particles was employed to obtain sheet images through the spherical flame balls. From these, areas of burned and unburned gas could be found and, from these, it was possible to derive the radius r_f. The mass burning rate turbulent velocity, u_t, was found from Eq. (10), with the density ratio found from [13].

Measured values of the variations of turbulent burning velocities with φ, for CH_4/air, with u'= 1m/s, at 300 K and 0.1MPa, from four different sources, are shown in Fig. 9. The bold solid curve shows the current values, from Eq. (10). The data from [14] and [16] are also from explosion flames, whilst the lowest values, [15], are from conical flames on cylindrical burners. with the turbulence generated by upstream by flow through perforated plates. With this steady state configuration there is no strong velocity pulse to generate further spatial rms turbulent velocities such as u_s', as is the case with the explosion flames. The higher values of u_t for the explosion flames in Fig. 9 can be explained by this mechanism. All the rigs were different and flames would have different flow patterns, and consequently, different modes of generating and dissipating turbulence.

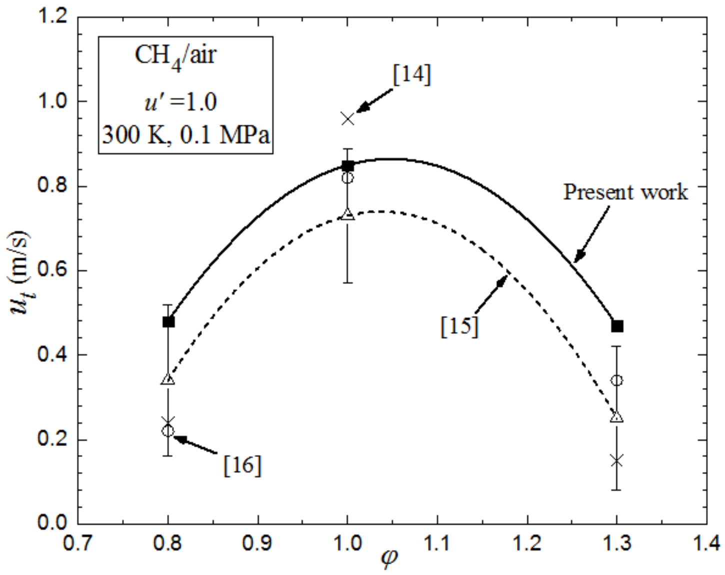

Fig. 9. Variation of u_t with φ. Burner measurements [15]. Others are explosions.

7. Conclusions

1. A fan-stirred explosion vessel, with a central region of good uniformity and isotropy has been employed to measure the mean and rms velocities ahead of explosion flames of CH_4/air.
2. As the initially small flame kernel grows into the full spectrum of turbulence length scales, on this count, the effective rms velocity acting on the flame front, u_k', increases, and this has been evaluated.
3. No turbulence generation was observed in explosions in the absence of initial turbulence.

4. With initial turbulence, the measured turbulence velocity u'_s, just ahead of the flame front increased during the explosion. This is termed the spatial rms turbulent velocity.
5. Part of the increase in u'_s, is due to the fuller active spectrum of turbulence, u'_k, see Figs. 1 and 8, with the remainder arising from further combustion-generated turbulence. Both u'_k and u'_s increase during an explosion, but that in u'_k is the greater.
6. The existing fan-stirred turbulence at the wrinkled flame front is enhanced by the high expansion velocity induced by combustion beyond that front.
7. This role of a high expansion velocity is confirmed experimentally, as is its generation by a combination of a high rate of combustion and a high increase in gaseous volume. Higher values of these parameters increase u'_s.
8. Isotropy and uniformity are difficult to achieve in many of the rigs employed for the measurement of turbulent burning velocities, u_t and the spatial distribution of the turbulence can affect the burning rate.
9. In Fig. 9 the lowest burning velocities were measured in burners with steady state conical flames, with no impulsive pulse to enhance the turbulence. As a result. explosion flames yielded higher, differing, values, and this is attributed to differences in the generation of u'_s.
10. The present results suggest that the principal factors enhancing the existing turbulence are a high burning velocity and a high gaseous expansion due to the combustion. In the generation of the turbulence by the velocity pulse, in all cases turbulence was already present. Bearing in mind that turbulent enhancement arises at the flame surface, another possibility is that it might also arise from wrinkling of the flame surface by thermo diffusive instabilities. Evidence for this possibility is provided in [17], which reports unstable mixtures with more negative Markstein numbers, generating Thermo Diffusive and Darius -Landau instabilities. These wrinkled the flames, causing a sudden acceleration in the burning rate and strong oscillations. However, the introduction of fan stirred turbulence reduced this effect as u'/u_l increased.

Acknowledgements

M.E.M thanks the University of Helwan for the academic support of his research.

References

1. Bradley, D., Lawes, M., Mansour, M., Flame surface densities during spherical turbulent flame explosions, Proc. Combust Inst., 32(1) (2009), 1587-1593. https://doi.org/10.1016/j.proci.2008.06.020.
2. Abdel-Gayed, R. G., Bradley, D., Lawes, M., Turbulent burning velocities: a general correlation in terms of straining rates, Proc. Royal Soc. Lond. 414 (1987), 389-413. https://doi.org/10.1098/rspa.1987.0150.
3. Gillespie, L., Lawes, M., Sheppard, C. G. W., Woolley, R., Aspects of laminar and turbulent burning velocity relevant to SI engines, SAE (2000), 13-33. https://www.jstor.org/stable/44634200.
4. Peters, N., Turbulent combustion. Cambridge University Press, 2000.
5. Lawes, M.. Effects of turbulence on combustion in engines. Ph.D. thesis, Uni. Leeds, 1987.
6. Bradley, D., Lawes, M., Morsy, M. E., Measurement of turbulence characteristics in a large scale fan-stirred spherical vessel, J. Turbulence, 20(3) (2019), 195-213. https://doi.org/10.1080/14685248.2019.1610566.
7. Morsy, M. E., Studies of Laminar and Turbulent Combustion Using Particle Image Velocimetry, PhD thesis, Uni. of Leeds, 2019. http://etheses.whiterose.ac.uk/id/eprint/25375.
8. Bradley, D., Lawes, M., Morsy, M. E., Flame speed and particle image velocimetry measurements of laminar burning velocities and Markstein numbers of some hydrocarbons, Fuel, 243(2019), 423-432. https://doi.org/10.1016/j.fuel.2019.01.067.
9. Borghi, R., 1985. On the structure and morphology of turbulent premixed flames. In Recent advances in the Aerospace Sciences, Plenum Press, New York. https://doi.org/10.1007/978-1-4684-4298-47.
10. P. Brequigny, C. Endouard, C. Mounaïm-Rousselle, F. Foucher, An experimental study on turbulent premixed expanding flames using simultaneously Schlieren and tomography techniques, Experimental Thermal and Fluid Science, 95, (2018) 11-17. https://doi.org/10.1016/j.expthermflusci.2017.12.018.

11. D. Bradley, M.Z. Haq, R.A. Hicks, T. Kitagawa, M. Lawes, C,G,W. Sheppard, R. Woolley, Turbulent burning velocity, burned gas distribution, and associated flame surface definition, Combust. Flame, 133 (2003) 415-430. https://doi.org/10.1016/S0010-2180(03)00039-7.
12. D. Bradley, M. Lawes, M. S. Mansour, The problems of the turbulent burning velocity, Flow Turbulence Combust. 87 (2011) 191-204.
13. C. Morley GasEq: a chemical equilibrium program for windows; 2005.
14. Shy, S. S., Lin, W. J., Wei, J. C., An experimental correlation of turbulent burning velocities for premixed turbulent methane-air combustion, Proc. Royal Soc. Lond. 456 (2000), 1997-2019.https://doi.org/10.1098/rspa.2000.0599.
15. Kobayashi, H., Seyama, K., Hagiwara, H., Ogami, Y., Burning velocity correlation of methane/air turbulent premixed flames at high pressure and high temperature, Proc. Combust. Inst. 30(2005), 827-834.https://doi.org/10.1016/j.proci.2004.08.098.
16. Muppala, S. P. R., Nakahara, M., Aluri, N. K., Kido, H., Wen, J. X., Papalexandris, M. V., Experimental and analytical investigation of the turbulent burning velocity of two-component fuel mixtures of hydrogen, methane and propane, Int. J. Hydrog. Energy, 34(2009), 9258-9265.https://doi.org/10.1016/j.ijhydene.2009.09.036.
17. S. AL-Shahrany, D. Bradley, M. Lawes, K. Liu, R. Woolley, Darrieus-Landau and thermo-acoustic instabilities in closed vessel explosions, Combust. Sci. and Tech., 178(2006) 1771–1802. https://doi.org/10.1080/00102200600788734.